Supporting Information

Martinez et al. 10.1073/pnas.1415460111

SI Text

Predictions from Magariyama and Kudo. We calculated the predicted dependence of swimming velocity on polymer concentration using the theory of Magariyama and Kudo (1) (Fig. S1) and show that, as they claimed, there is a peak. However, we also show a calculation that they did not report, namely, the predicted dependence of body rotation frequency as a function of polymer concentration. The latter is a rapidly increasing function, which is clearly unphysical and contradicts the observation by BT (2), as well as data shown here (Fig. 4).

Characterizing the PVP.

Intrinsic viscosity and overlap concentration. The viscosity of a polymer solution at low concentrations can be written as a virial expansion of η in c

$$\eta = \eta_s\left(1 + [\eta]c + k_H[\eta]^2c^2 + \ldots\right), \qquad \text{[S1]}$$

where $[\eta]$ and k_H are the intrinsic viscosity and the Huggins coefficient, respectively, and η_s is the viscosity of the solvent, which here is motility buffer. The linearity at low c can be expressed in two different ways

$$\frac{\eta - \eta_s}{\eta_s c} = [\eta] + k_H[\eta]^2 c \quad \text{(Huggins)}, \qquad \text{[S2]}$$

$$\frac{\ln(\eta/\eta_s)}{c} = [\eta] + \left(k_H - \frac{1}{2}\right)[\eta]^2 c \quad \text{(Kraemer)}. \qquad \text{[S3]}$$

These two linear plots should extrapolate to $[\eta]$ at $c = 0$. The intrinsic viscosity measures the volume of a polymer coil normalized by its molecular weight, so that $c^* \approx [\eta]^{-1}$. A modern text names this as the best experimental method for estimating the overlap concentration (3).

We first regraph the $\eta(c)$ data given by SD (4) as HK plots (Fig. S2*A*). For here and below, concentrations in wt% and grams per deciliter are interchangeable at the sort of concentrations we are considering. It is clear that their lowest c data point must be inaccurate. Discarding this point gives the expected linear dependence in both plots and a uniquely extrapolated value of $[\eta] = 1.055$ at $c = 0$, giving $c^* = 0.95$ g/dL. Reference to our c^* values below suggests that SD's PVP360k has somewhat lower molecular weight than our material with the same label.

According to current industry standards (5), PVP360k should have viscosities of ≈3–5 and ≈300–700 mPa·s at 1 and 10 wt.% in water, respectively. SD's reported viscosities at 1 and 10 wt.% at 2.5 and 249 Pa·s, respectively, are lower than these values, again consistent with their material having lower molecular weight than our PVP360k.

We characterized all four PVPs used in this work by measuring their low-shear viscosity in motility buffer as a function of concentration. For PVP360k (K-90) at 1 and 10 wt.%, we found $\eta \approx 4$ and 370 mPa·s, agreeing well with the published standards (5). We now graph the measured viscosities of our four PVPs at low concentrations as HK plots (Fig. S2 *B*–*E*). In each case, the expected behavior is found; the extrapolated values of $[\eta]$ and the overlap concentrations calculated from these are given in Table S1. The scaling of $[\eta]$ vs. M is consistent with a power law (Fig. S2*F*) $[\eta] \sim M^a$, with $a = 0.781$. Because $[\eta] \approx r^3/M$, $r \sim M^\nu$ with $\nu = (1+a)/3$. We find $\nu = 0.593$, which is consistent with the renormalization group value of $\nu = 0.588$ for a linear polymer in a good solvent.

Coil radii, second virial coefficient, and molecular weight. We performed static and dynamic light scattering (SLS and DLS, respectively) experiments to measure the radius of gyration, R_g, the molecular weight, M_w, the second virial coefficient, A_2, and the hydrodynamic radius, R_h, of PVP360k in water and motility buffer (6). R_h was measured by DLS, and R_g, M_w, and A_2 were measured using the Zimm plot of SLS data. Results are summarized in Table S2. The positive A_2 is consistent with our conclusion above that water is a good solvent for PVP. There may be a mild degree of aggregation in motility buffer (larger radii and slightly smaller A_2).

Native Polymer Results. Fig. S3*A* shows $\bar{v}$ and $\overline{\Omega}$ vs. polymer concentration, c, for as-bought, or native, PVP360k. Although $\overline{\Omega}(c)$ decays monotonically, a peak is observed in $\bar{v}$ at $c \approx 0.5$wt%, or roughly c^* for this molecular weight. The latter ostensibly reproduces SD's observations (4): their data are also plotted in Fig. S3*A*. In native PVP160k (Fig. S3*B*), the peak in $\bar{v}(c)$ broadens, and now there is a corresponding broad peak in $\overline{\Omega}(c)$ as well. These peaks broaden out into plateaus for native PVP40k and PVP10k (Fig. S3 *C* and *D*). We also performed experiments with native Ficoll with the manufacturer-quoted molecular weights of 70k and 400k and observed similar nonmonotonic, broadly peaked responses in both $\bar{v}(c)$ and $\overline{\Omega}(c)$ (Fig. S4).

The Effect of Small-Molecule Energy Sources. Here we show $\bar{v}(c)$ for *E. coli* swimming in glycerol solutions of a range of concentrations (Fig. S5). The plot is indeed reminiscent of what is seen for native PVP10k and PVP40k. Indeed, we suggest that the increases at low concentrations in all four polymers have the same origin as the increase observed at low glycerol concentration: the availability of a small-molecule energy source. The decrease at high glycerol is an osmotic effect (as observed for other small molecules, e.g., sucrose) (7), whereas that seen in the 10k, 40k, and 160k polymers can be entirely accounted for by low-Re Newtonian hydrodynamics (polymeric osmotic effects at our concentrations are negligible).

Dialyzed Ficoll Results. Swimming speed and body rotation frequency as a function of concentration are shown for two purified Ficolls in Fig. S6.

Shear-Thinning Calculations.

Predicting Ω(v) for flagellum experiencing buffer viscosity. Here we outline the procedure used to calculate the rotation rate of the cell body for a bacterium swimming in shear-thinning PVP360k solution as a function of the swimming speed. We assume that the flagellum sees a viscosity η' that is different from the low-shear-rate viscosity η experienced by the bacterial body. This assumption is partly motivated by bulk and microrheological measurements (Fig. 6), showing that at the shear rates generated by the flagellum, shear thinning can be expected at least down to the micrometer scale. Empirically, the low- and high-shear viscosities plotted in Fig. 6 can be fitted by

$$\begin{cases} \eta_{\text{low-shear}} = -5.32 + 6.33\exp(0.39c) & \dot{\gamma} \to 0\,s^{-1}, \\ \eta_{\text{high-shear}} = 0.96 + 0.69c + 0.44c^2 & \dot{\gamma} = 10^4\,s^{-1}, \end{cases} \qquad \text{[S4]}$$

where c is in wt% and η in centipoise (cP).

In this two-viscosity model, the force and torque balance equations solve to Eq. **13**

$$\frac{\Omega}{v}=\frac{\hat{d}\left[\left(\frac{\eta}{\eta'}\right)\hat{a}_0+\hat{a}\right]-\hat{b}^2}{\left(\frac{\eta}{\eta'}\right)\hat{d}_0\hat{b}}. \quad [S5]$$

The friction coefficients in Eq. **S5** are given by (8)

$$\hat{a}=k_nL\sin\psi\tan\psi\left(1+\gamma\cot^2\psi\right), \quad [S6]$$

$$\hat{b}=k_nL\frac{\lambda}{2\pi}\sin\psi\tan\psi(1-\gamma), \quad [S7]$$

$$\hat{d}=k_nL\left(\frac{\lambda}{2\pi}\right)^2\sin\psi\tan\psi\left(1+\gamma\cot^2\psi\right), \quad [S8]$$

$$\hat{a}_0=\frac{4\pi b}{\ln\frac{2b}{a}-\frac{1}{2}}, \quad [S9]$$

$$\hat{d}_0=\frac{16\pi}{3}a^2b, \quad [S10]$$

where

$$k_n=\frac{8\pi}{2\ln\frac{c\lambda}{r}+1}, \quad [S11]$$

$$k_t=\frac{4\pi}{2\ln\frac{c\lambda}{r}-1}, \quad [S12]$$

and $\gamma=k_t/k_n$. Here, $L=7$ μm and $\lambda=2$ μm are the total length and pitch of the flagellum, respectively, $\psi=41^\circ$ is the angle made by the flagellar filament with the flagellar axis, $r=20$ nm is the estimated radius of the composite filament in a flagella bundle, and $c=2.4$ is the Lighthill constant. All parameters are taken from a previous experimental paper (8), where this set of parameters were shown to be consistent with the Purcell model.

Using the measured values of $\overline{\Omega}(c)$ for PVP360k, $\eta'=\eta_s$, $\eta=\eta_{\text{low-shear}}$, and Eq. **S5** is sufficient to calculate the corresponding $\overline{v}(\overline{\Omega})$. Results show good agreement with the measured values (Fig. 3), thus predicting a peak in the swimming velocity on an increase in the viscosity of the polymer solution. For a better illustration, we compare the predicted and measured values of $\overline{v}$ as a function of the viscosity experienced by the body ($\eta_{\text{low-shear}}$) in Fig. S7. Our theory is successful in predicting a peak in the swimming velocity in the right position and of the right shape.

Deducing the viscosity the flagellum sees from measurements. Now we relax our previous assumption that η' is equal to the viscosity of the solvent, and use Eq. **S5** to extract the viscosity of the fluid surrounding the flagellar filament. Using the measured values of $\overline{\Omega}(c)$ and $\overline{v}(c)$, Eq. **S5** can be solved for η'. The results are shown in Fig. 6. Indeed, for most of the concentration range studied, $\eta'\approx\eta_s$.

Dark-Field Flicker Microscopy. Under dark-field illumination, the image of a swimming bacterium appears to flicker. By calculating the power spectrum of the spatially localized time-dependent intensity fluctuations of low-magnification images of a quantized pixel box (containing approximately one cell) and then averaging over all cells in the images, we are able to measure the body rotational frequency $\Omega/2\pi$ averaged over $\sim10^4$ cells based on a $\lesssim$ 10-s movie. This method is similar to what was done by Lowe et al. (9), who measured the power spectrum of single swimming cells. However, here we use low-magnification dark-field imaging, which allows high-throughput measurement of $\Omega/2\pi$.

Dark-field movies were recorded (Nikon Plan Fluor 10×Ph1 objective, NA = 0.3, Ph3 phase-contrast illumination plate) at either 500 or 1,000 Hz on an inverted microscope (Nikon TE300 Eclipse) with a Mikrotron high-speed camera (MC 1362) and frame grabber (Inspecta 5, 1-Gb memory) at room temperature (22 ± 1 °C). The images correspond to an area of $\approx720\times720$ μm, containing around 10^4 bacteria. Approximately 4,000 frames were captured, at a resolution of 512 × 512 pixels.

To process a video sequence, each frame was divided into square tiles of side length l (typically five pixels), and the pixel values in each tile were summed to give a single number. This process was repeated for every frame in the video sequence, yielding intensity as a function of time for each tile. The power spectrum of these data was calculated for each tile separately, before averaging over all tiles to give smoothed data for the whole video sequence. The power spectrum is then normalized by the frequency squared to remove any contribution from Brownian motion due the nonmotile cells, inherently present in the bacterial suspensions. An example is shown in Fig. S9. We identify the first peak as the body rotational frequency $\Omega/2\pi$ in line with previous studies (9).

Viscosity Measurements. The viscosity of PVP360k measured using conventional rheometry and DWS microrheology (*Materials and Methods*) at different concentrations is shown in Fig. S8. There is reasonable overlap between the two methodologies at intermediate shear rates.

1. Magariyama Y, Kudo S (2002) A mathematical explanation of an increase in bacterial swimming speed with viscosity in linear-polymer solutions. *Biophys J* 83(2):733–739.
2. Berg HC, Turner L (1979) Movement of microorganisms in viscous environments. *Nature* 278(5702):349–351.
3. Rubinstein M, Colby RH (2003) *Polymer Physics* (Oxford Univ Press, Oxford, UK).
4. Schneider WR, Doetsch RN (1974) Effect of viscosity on bacterial motility. *J Bacteriol* 117(2):696–701.
5. Bühler V (1998) *Kollidon: Polyvinylpyrrolidone for the Pharmaceutical Industry* (BASF, Ludwigshafen, Germany), 4th Ed.
6. Berne BJ, Pecora R (2000) *Dynamic Light Scattering* (Dover Publications, New York).
7. Pilizota T, Shaevitz JW (2013) Plasmolysis and cell shape depend on solute outer-membrane permeability during hyperosmotic shock in E. coli. *Biophys J* 104(12): 2733–2742.
8. Chattopadhyay S, Moldovan R, Yeung C, Wu XL (2006) Swimming efficiency of bacterium Escherichia coli. *Proc Natl Acad Sci USA* 103(37):13712–13717.
9. Lowe G, Meister M, Berg HC (1987) Rapid rotation of flagellar bundles in swimming bacteria. *Nature* 325(2):637–640.

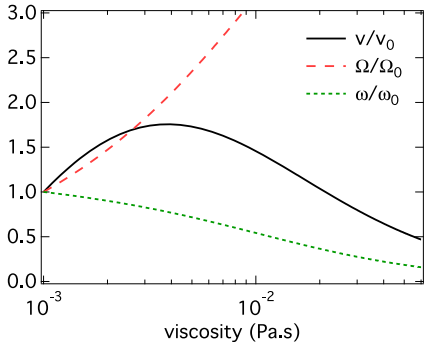

Fig. S1. Normalized swimming speed v/v_0, body rotational speed Ω/Ω_0, and flagella rotational speed ω/ω_0 vs. viscosity according to Magariyama and Kudo (1).

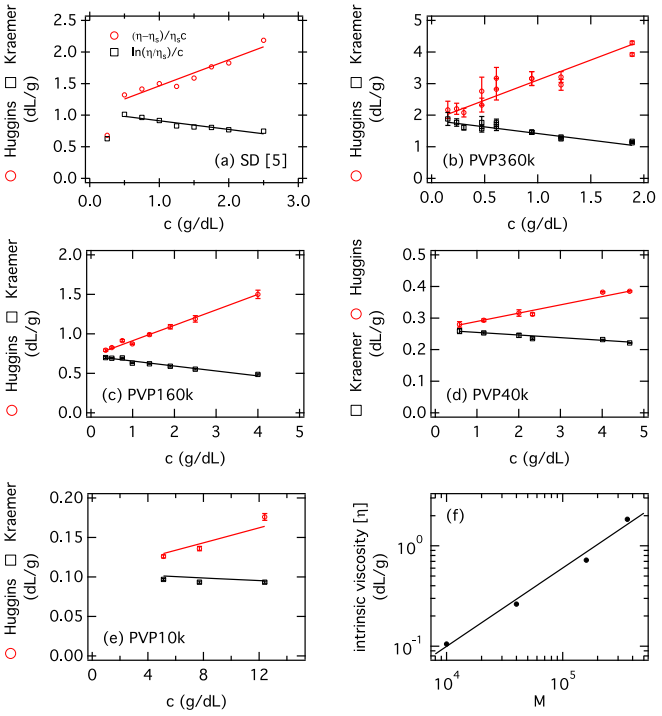

Fig. S2. (*A*–*E*) Huggins and Kraemer representation: (red circles) $(\eta-\eta_s)/\eta_s c$ and (black squares) $\ln(\eta/\eta_s)/c$ vs. polymer concentration. Lines are linear fits to the data using Eqs. **S2** and **S3** simultaneously. Both quantities should be linear and extrapolate to a unique intrinsic viscosity $[\eta]$ at $c=0$. (*A*) From the PVP viscosity data of Schneider and Doetsch. Discarding the lowest-*c* point gives $[\eta]=1.05\pm0.02$. (*B*–*E*) Our PVP at four different molecular weights. (*F*) The scaling of intrinsic viscosity, $[\eta]$, with molecular weight, *M*, for our PVPs.

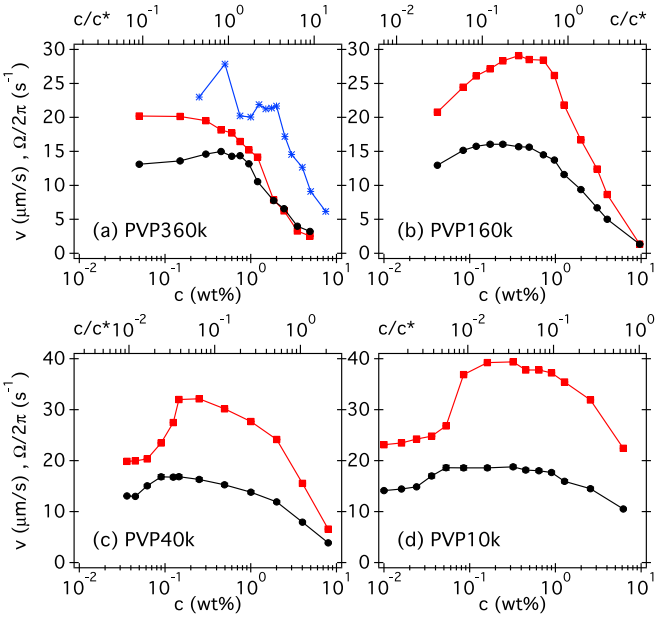

Fig. S3. (*A–D*) Swimming speed $\overline{v}$ (black circles) and body rotation frequency $\overline{\Omega}/2\pi$ (red squares) of *E. coli* vs. concentration (in weight percent) of native PVP of four molecular weights. Top axis: PVP concentration normalized to the overlap concentration c* (see Table S1). The stars (blue) in *A* are results for swimming speed from SD (4).

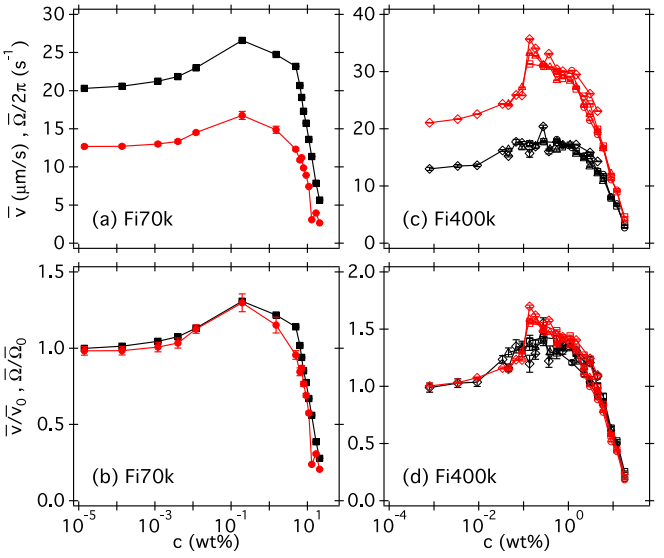

Fig. S4. Speed $\overline{v}$ (red symbols) and body rotation frequency $\overline{\Omega}$ (black symbols) given in absolute (*Upper*) and normalized values (*Lower*) as functions of concentration for native Ficoll of two molecular weights: (*A* and *B*) $M = 70$k (one dataset) and (*C* and *D*) $M = 400$k (four datasets). Lines are guides to the eye.

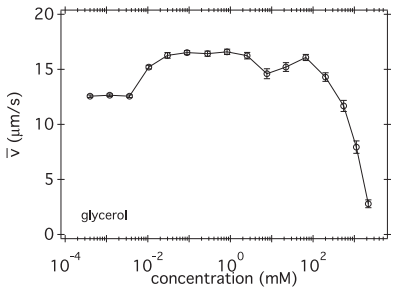

Fig. S5. Swimming *E. coli* in glycerol. Speed $\overline{v}$ as a function of glycerol concentration.

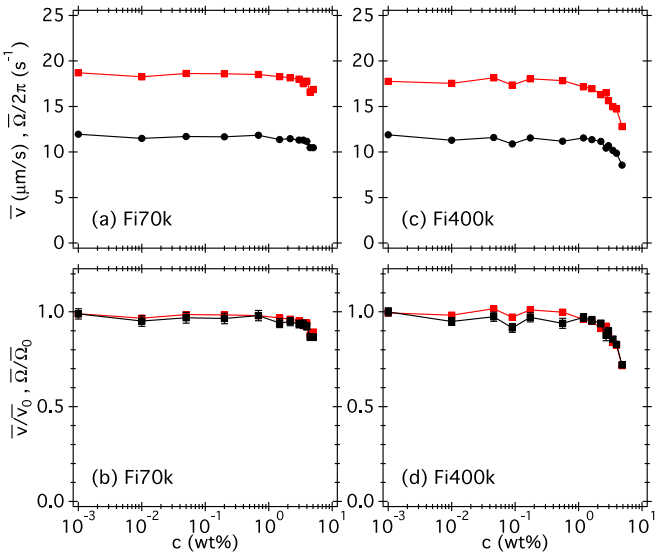

Fig. S6. Speed $\overline{v}$ (red circles) and body rotation frequency $\overline{\Omega}$ (black squares) given in absolute (*Upper*) and normalized values (*Lower*) as functions of concentration for dialyzed Ficoll of two molecular weights: (*A* and *B*) M = 70k and (*C* and *D*) M = 400k. Lines are guides to the eye.

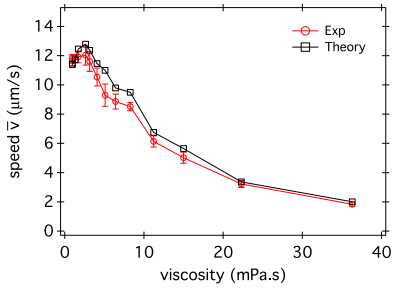

Fig. S7. Speed $\overline{v}$ vs. viscosity from experiments (black dots) and our theory (red diamonds) as discussed in *SI Text*.

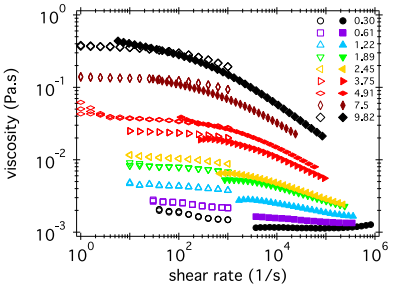

Fig. S8. Viscosity of PVP360k as a function of shear rate obtained from bulk rheology (open symbols) and DWS microrheology (filled symbols) for several polymer concentrations (see legend in weight percent).

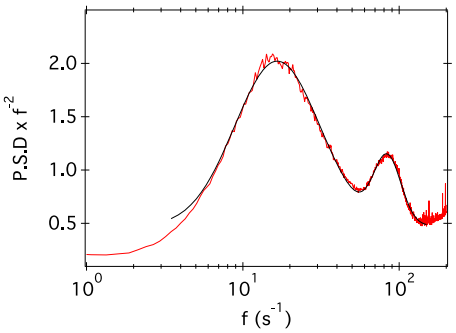

Fig. S9. Typical example of the power spectrum of the flickering dark-field image of individual cells averaged over $\approx 10^4$ cells based on an $\approx$10-s dark-field movie (*Materials and Methods*). The power spectrum is normalized by the frequency square to remove contribution from Brownian motion due to the inherent presence of nonmotile cells in the suspension. The black line corresponds to a two-peak fit using Lognormal distribution.

Table S1. Intrinsic viscosity, [η], and Huggins coefficient, k_H, obtained by fitting simultaneously (global fitting) the viscosity data using both Huggins and Kraemer equations

Solutions	$[\eta]$ (dL/g)	k_H	c^*(g/dL or wt%)
PVP360k	1.84 ± 0.04	0.38 ± 0.02	0.55 ± 0.01
PVP160k	0.72 ± 0.01	0.38 ± 0.01	1.40 ± 0.02
PVP40k	0.263 ± 0.003	0.38 ± 0.02	3.8 ± 0.1
PVP10k	0.105 ± 0.006	0.42 ± 0.08	9.5 ± 0.5
SD (4)	1.05 ± 0.02	0.38 ± 0.02	0.95 ± 0.02

Table S2. Parameters obtained from SLS and DLS for PVP360k in water or in motility buffer (MB)

Solutions	M_w (g/mol)	A_2 (mol L/g^2)	R_g (nm)	R_h (nm)
PVP360k in water	840×10^3	3.0×10^{-7}	56	30
PVP360k in MB	$1{,}500 \times 10^3$	2.6×10^{-7}	79	37